Multi-State Dynamic Pathways for Anisotropic Colloidal Assembly & Reconfiguration

Rachel S. Hendley, Lechuan Zhang, and Michael A. Bevan* Chemical & Biomolecular Engineering, Johns Hopkins University, Baltimore, MD 21218, USA

Abstract

We report controlled interfacial assembly and reconfiguration of rectangular prism colloidal particles between microstructures of varying positional and orientational order including stable, metastable, and transient states. Structurally diverse states are realized by programming time dependent electric fields that mediate dipolar interactions determining particle position, orientation, compression, and chaining. We identify an order parameter set that defines each state as a combination of positional and orientational order. These metrics are employed as reaction coordinates to capture microstructure evolution between initial and final states upon field changes. Assembly trajectory manifolds between states in the low-dimensional reaction coordinate space reveal a dynamic pathway map including information about pathway accessibility, reversibility, and kinetics. By navigating the dynamic pathway map, we demonstrate reconfiguration between states on minute timescales, which is practically useful for particle-based materials processing and device responses. Our findings demonstrate a conceptually general approach to discover dynamic pathways as a basis to control assembly and reconfiguration of self-organizing building blocks that respond to global external stimuli.

keywords: self-assembly | low dimensional models | reaction coordinate trajectories | rectangular prism particles | induced dipolar potentials

Introduction

Knowledge of self-assembly mechanisms is essential to understand the spatiotemporal emergence of structures and functions in diverse biological (e.g., proteins, viruses, membranes, cells) and synthetic (e.g., molecules, macromolecules, nanoparticles, colloids) material systems. ¹⁻² A key challenge is to understand how building block interactions determine rate limiting transition and metastable states along pathways towards target states to determine the time evolution of self-assembly processes. ³⁻⁶ From a technological viewpoint, such mechanistic information can enable informed intervention in the quantitative design, control, and optimization of self-assembly for material properties and processing. ⁷⁻⁹ Despite the importance of understanding self-assembly mechanisms for many distinct materials and applications, significant challenges remain for the connected tasks of designing experiments to interrogate essential mechanisms and developing minimally complex dynamic models that capture dominant features.

Colloidal self-assembly is amenable to exploration of mechanistic details including dynamic pathways based on the capability for real-space and real-time particle tracking and tunable interactions (*e.g.*, steric, ¹⁰⁻¹¹ depletion, ¹²⁻¹³ induced dipoles, ¹⁴⁻¹⁶ DNA binding, ¹⁷⁻¹⁸ etc.). Colloidal assembly has clear technological importance given the prevalence of colloidal particles in numerous consumer products, natural biological and environmental systems, ¹⁹⁻²⁰ and emerging advanced particle based materials and devices. ²¹⁻²⁴ Different shaped colloidal building blocks have

Hendley et al. Page 1 of 22

^{*}Corresponding author: mabevan@jhu.edu

the potential to yield many different useful multifunctional microstructures in bulk 3D materials²⁵ and in 2D surface coatings.²⁶⁻²⁷ However, colloidal assembly pathways have been demonstrated in a limited number of simulation studies (*e.g.*, see representative examples²⁸⁻³²) and even fewer experimental studies where obtaining necessary spatiotemporal resolution and statistics is challenging. Examples of experimental investigations quantifying dynamic pathways include studies of spherical colloids undergoing crystal nucleation,³³ grain boundary formation and motion,³⁴ small cluster rearrangements,³⁵ and crystal order-order transitions.³⁶ Spherical colloidal crystal assembly has minimal complexity compared to many self-assembling systems (*e.g.*, number of states & pathways), but the simplicity has enabled relatively complete mechanistic understanding captured in high dimensional simulations, low dimensional dynamic models, and even optimal feedback control of self-assembly processes.³⁷⁻⁴⁰

Perhaps the most challenging aspect of defining colloidal assembly dynamic pathways, and self-assembly mechanisms in general, is simultaneously determining the number of dynamic processes (*i.e.*, dimensionality⁴¹) and a set of physically meaningful metrics to quantify their trajectories (*i.e.*, reaction coordinates³⁴). The difficulty of determining dimensionality and reaction coordinates has been described as a "chicken-and-egg problem" and as requiring a "procedure for having an epiphany"; these statements refer to the lack of *a priori* methods for simultaneous dimensionality reduction/reaction coordinate identification and recognize the current state-of-the-art *a posteriori* approach that essentially requires intuition and iteration by domain experts. Once the dimensionality and reaction coordinates are known, it is possible to discover mechanistic dynamic pathways (*e.g.*, free energy landscapes), ³¹ stochastic structure evolution between states (*e.g.*, first passage times), and optimal control algorithms (*e.g.*, dynamic programming). ^{37, 39-40} Our prior studies of colloidal crystallization (*e.g.*, refs^{31, 34, 37-41}) employed dimensionality reduction to aid analysis and validate findings, but we are unaware of *a priori* dimensionality reduction/reaction coordinate identification methods to initialize studies of previously uncharted colloidal self-assembly problems. ³⁸

Increasingly complex building blocks yield a desirable abundance of microstructural configurations with exceptional optical, electrical, mechanical, thermal, wetting, and other emergent material properties/behaviors (too numerous to summarize here, but catalogued in representative reviews).^{7-9, 25, 42-43} However, different shaped colloids with increased degrees of freedom inherently have additional dynamical complexity in their assembly mechanisms, and tend to yield defective ordered states or more commonly arrested amorphous states.⁴⁴⁻⁴⁵ External fields can increase the number of states and improve the degree of liquid crystalline ordering of anisotropic colloids, ⁴⁶⁻⁴⁸ but such states are still relatively slow to form and suffer from a variety of topological defect types.⁴⁹⁻⁵¹ Anisotropic particle reconfiguration between multiple states has not generally been explored in detail beyond two-state isotropic-nematic and isotropic-crystal transitions⁵²⁻⁵⁴ and application to diverse shapes is still in development. Because AC electric fields can induce dipolar interactions in essentially any particle material, shape, and size,⁵⁵ approaches to field mediated assembly can be material agnostic and applicable to diverse applications.

Recently, we have shown for a class of convex superelliptical prism particles (e.g., disks, ellipses, squares, rhombuses, rectangles, rounded variants, etc.) how AC electric field mediated dipolar interactions together with packing effects (entropy) yield diverse liquid crystal and crystalline states. ²⁶⁻²⁷ A key aspect of achieving these states was the ability to tune kT-scale dipolar potentials (via field voltage, frequency), ⁵⁶⁻⁵⁷ where the thermodynamic driving force and system state are well defined. Changing kT-scale potentials in an informed manner can be used to perturb

Hendley et al. Page 2 of 22

a system out of equilibrium, where it subsequently re-equilibrates via stochastic microstructure evolution (drift and diffusion) on a different free energy landscape. In contrast, abruptly changing >>kT interactions often leads to amorphous arrested or aggregated states (via rapid drift), where diffusive motion that drives self-assembly vanishes and relaxation/reconfiguration is irreversibly quenched. As a result, understanding how changing kT-scale interactions determine dynamic pathways is necessary to engineer self-assembly and reconfiguration processes that occur on reasonable timescales and do not terminate in trivial arrested, irreversible, amorphous states.

Despite prior investigations of many aspects of anisotropic particle self-assembly, we are unaware of studies estimating dimensionality, reaction coordinates, or dynamic pathways for assembly of different shaped colloidal particles in experiments (simulations have probed limited aspects⁵⁸). Although the simplest model systems of spherical colloids have been understood in terms of low dimensional dynamic pathway models,^{28, 33} consideration of additional complexity in terms of shape anisotropy has received little attention. From a broader perspective, a similar issue is encountered in many self-assembling systems – for example, where peptides are generally investigated rather than complete proteins – complexity often increases too quickly (*i.e.*, "curse of dimensionality"). Ultimately, there are quite a few open questions and challenges related to extending approaches for quantifying stochastic evolution of self-assembling building blocks to increasingly complex systems, with important scientific and technological impacts.

Here, we investigate non-equilibrium dynamic pathways for self-assembly of rectangular prism shaped particles into diverse microstructures within quasi-2D monolayers in AC electric fields (Fig. 1). These experiments probe well defined states and conditions from knowledge of how AC electric field amplitude and frequency mediate shape-dependent dipolar interactions, ²⁶ particle positions and orientations,⁵⁶ and packing under compression.^{26-27, 59-60} Furthermore, as a foundation for probing non-equilibrium dynamics in this system, we have identified for quasi-twodimensional rectangular prism particles the equilibrium phases of hard particles²⁶ and accessible metastable states in AC electric fields.²⁷ These prior studies uncovered a diversity of transient, metastable, defective, and stable states, that indicated greater complexity in the non-equilibrium states and dynamical behavior compared to other 2D particle shapes. The rectangular prism particle anisotropy together with the presence of corners stabilizes a number of liquid crystal states and can influence slow dynamics via translation-rotation coupling. In the following, we first identify a number of states of interest in optical microscopy experiments. We next determine a minimal set of reaction coordinates, and hence dimensionality, to define states and dynamic pathways as manifolds of stochastic assembly trajectories between different initial and final states based on dipolar potential changes. Finally, we use the resulting dynamic pathway map to navigate and reconfiguration between all states on diffusion limited timescales, which is practically useful for viable materials processing times and device response rates.

Results & Discussion

Field Mediated Anisotropic Particle Assembly

Non-uniform AC electric fields induce dipoles on different shaped colloidal particles via polarization of their electrostatic double layers, which can be used to control their position, orientation, and concentration within quasi-2D monolayers between thin film electrodes (**Fig. 1A**). For the rectangular prism particles investigated in this work (axis dimensions of $8.4 \times 4.6 \times 1.6 \mu m$), 12 possible states of single particle positions and orientations can be achieved by controlling the electric field amplitude and frequency. We focus on the case where the induced

Hendley et al. Page 3 of 22

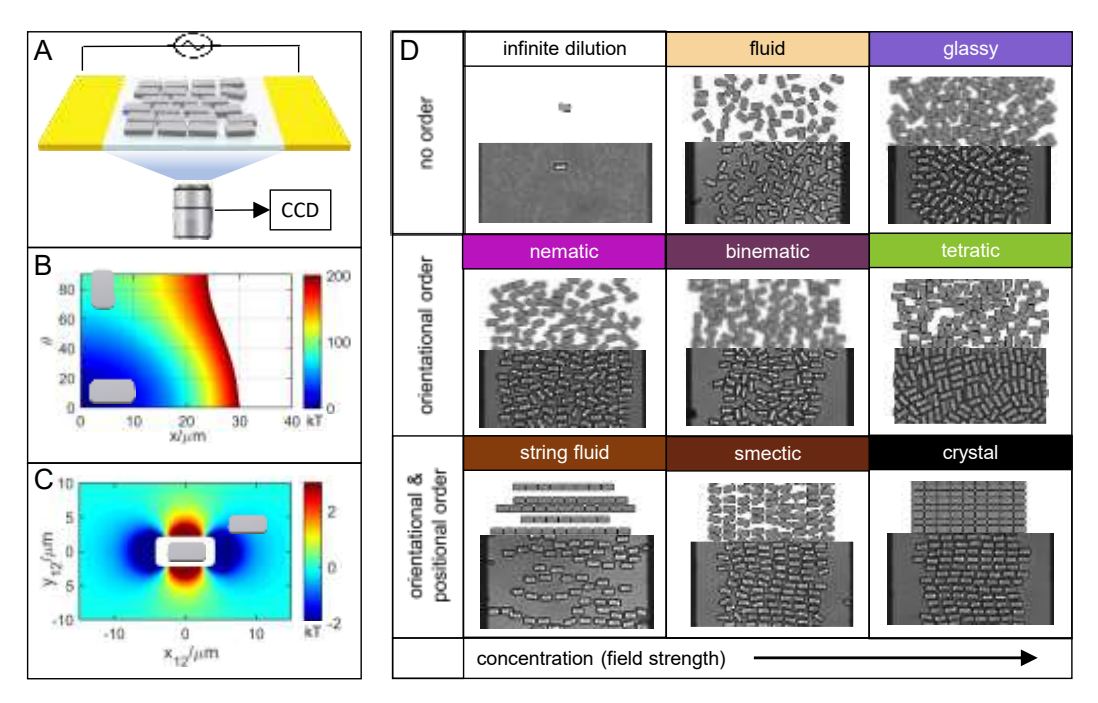


Fig. 1. Microscopy electrode cell, dipolar potentials, and assembled states of rounded rectangles. (**A**) Schematic of optical microscopy cell for observing quasi-2D monolayers of rounded rectangular colloids between 100 μm coplanar electrodes to generate AC electric fields. Potential energy landscapes for: (**B**) position and orientation dependence of induced dipoles in nonuniform electric field at the electrode gap center (dipole-field potential⁵⁶), and (**C**) relative position dependent interaction between induced dipole pairs (dipole-dipole potential⁵⁷). (**D**) States of assembled rectangles in renderings and images organized by degree of orientational and position order and average concentration. Photolithographic epoxy particle dimensions are: $2r_x = 8.4 \mu m$, $2r_y = 4.6 \mu m$, and $2r_z = 1.6 \mu m$ and provide internal image scale bar.

dipole-field potential has a potential energy minimum (Fig. 1B) corresponding to a particle position at the electric field minimum at the electrode center, and an orientation with the long axis aligned with the field and the smallest axis perpendicular to the substrate. Particle translation and rotation out of the plane parallel to the substrate are minimal based on confinement by gravity and electrostatic repulsion between the particle and glass microscope slide.

An ensemble of dipolar particles can be compressed at the electric field minimum, where induced dipole-field interactions continue to influence particle position and orientation, but dipole-dipole potentials (**Fig. 1C**) and particle packing effects (similar to corresponding hard particle shapes²⁶) also contribute to the net balance of interactions determining the particle configuration within quasi-2D monolayers.⁵⁷ Because non-uniform fields compresses dipolar particles against their osmotic pressure,^{57, 61} field amplitude can partly be considered as an analog of pressure. In addition, because particle polarizability along different axes relative to the medium depend on field frequency, frequency selection determines whether particles concentrate at field maxima or minima and which particle orientation has the lowest energy.^{56, 62} As a result, the AC electric field amplitude and frequency together provide some control authority over both particle position and orientation within concentrated particle ensembles.

2D Rectangular Prism Particle States

The balance of field mediated interactions and particle packing effects in the nonuniform AC electric field leads to a number of quasi-2D states (**Fig. 1D**). State classification and nomenclature is based on prior studies of rectangular⁵⁹⁻⁶⁰ and dipolar¹⁴⁻¹⁶ particles, which are

Hendley et al. Page 4 of 22

summarized in our prior studies of superelliptical prism particle states.²⁶⁻²⁷ States are characterized by their degree of orientational and positional order within liquid, liquid crystalline, and crystalline microstructures. Representative optical microscopy images and renderings show accessible states of ~140-220 particles. We characterize these states as fluid, glassy, nematic, binematic, tetratic, string-fluid, smectic, and 4-fold ordered crystals. These states are expected based on our prior studies of the same shape particles with hard interactions having equilibrium fluid, nematic, and crystal phases (in simulations),²⁶ and with field induced dipolar interactions and confinement exhibiting fluid, nematic, tetratic, smectic, and crystalline states (in experiments).²⁷

Stable fluid, nematic, and crystal states correspond to equilibrium phases in large uniform systems, whereas metastable states appear as types of defective, transient, or arrested states. The "binematic" state, using previously defined nomenclature, ⁶⁰ indicates a nematic state with a portion of misoriented particles (generally orthogonal to the nematic director). The binematic state is intermediate to nematic states with all particles having uniaxial alignment along a single director, and tetratic states with an equal number of particles oriented along orthogonal directors (*i.e.*, biaxial orientational order). We detect evidence of transient smectic states with one-dimensional positional order (layering along a nematic director). A string fluid state is observed, which consists of dipolar particles chains in head to tail configurations along the particle long axes. This state is similar to dipolar chains of spherical colloids, ¹⁴⁻¹⁶ which can percolate between electrodes to modulate circuit impedance. Rapid quenches of fluid states produce "glassy" states having minimal positional or orientation order like fluids, but with signatures of dynamic arrest (*e.g.*, dynamical heterogeneity, lack of long time self-diffusion, slow aging, etc.). ⁴⁴⁻⁴⁵ In the following, we discuss order parameters to define states from particle coordinates, which we subsequently use as reaction coordinates to monitor microstructure evolution and relaxation between states.

Order Parameters & States

We identify a minimal number and types of order parameters to capture the observed states based on instantaneous configurations in microscopy or computer experiments. The aim is to monitor order parameters vs. time as reaction coordinates for dynamic assembly and reconfiguration processes. A minimal order parameter set that capture all stable states as well as defective, transition, and metastable states can provide a low dimensional model of dynamic pathways on free energy landscapes. Identifying the minimal number and correct order parameters is nontrivial, but can be aided by dimensionality reduction methods. In the following, we describe a minimal set that appears to capture the key states and transitions between them, although further exploration could yield alternate metrics distinguishing states and critical microstructural features along pathways.

Here we demonstrate a combination of three order parameters to identify states of interest (**Fig. 1**). The three parameters are: (1) the average local nematic order (S_2), the average local tetratic order (T_4), and the average local stretched four-fold connectivity (C_4 , combining 4-fold bond orientational order and coordination number), where each parameter takes values between 0 and 1 and is defined in **Methods**. These order parameters are well established based on their global variants for determining equilibrium phases of 2D rectangles^{26, 59-60} and related metrics for metastable states in related systems of disks, spheres, ellipses, and rectangles. Averaging each local order parameter over all particles in a given configuration provides an effective global order parameter for that state. Global nematic, tetratic, and 4-fold connectivity parameters were previously shown to capture stable states of nearly rectangular hard prisms with and without fields. However, average local order parameters better capture emergence of local order and

Hendley et al. Page 5 of 22

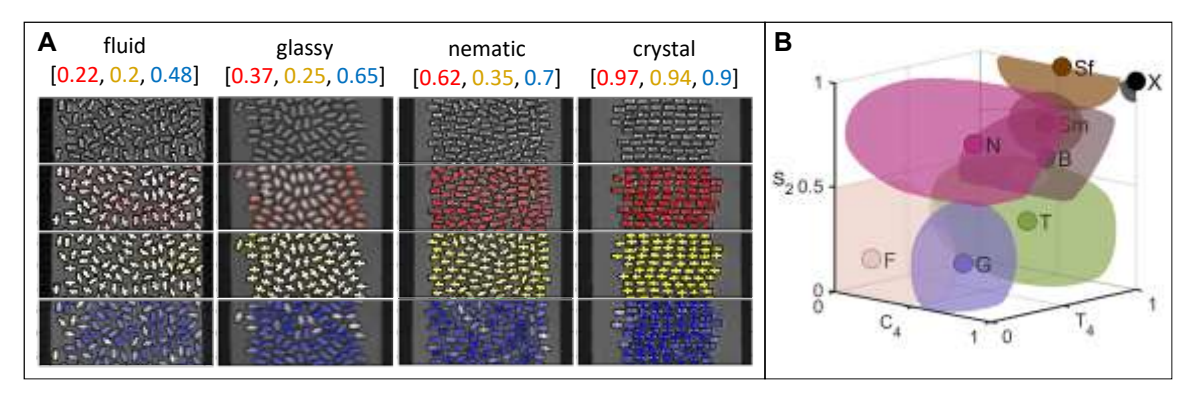


Fig. 2. Order parameters and reaction coordinates for assembled rectangle states. (**A**) States of rectangles in (left-to-right) fluid, glassy, nematic, and crystal configurations in AC electric fields. Particles individually colored by $S_{2,i}$ (red, Eq. (1)), $T_{4,i}$ (yellow, Eq. (2)) and $C_{4,i}$ (blue, Eq. (3)). (**B**) 3D state map to indicate regions for microstructures in Fig. 1 with states (abbreviations) as: fluid (F), nematic (N), crystal (X), glassy (G), binematic (B), string fluid (Sf), smectic (Sm), and tetratic (T). Coloring scheme includes average S_2 , T_4 , and C_4 ranging from white to red, white to yellow, or white to blue from 0 to 1. Colors are mixed such that [0, 0, 0] corresponds to white and [1, 1, 1] is black.

its evolution into global order by capturing defects, spatial variations, and edge effects within the non-uniform, non-equilibrium, and small systems in the present work (similar to our past work on spherical colloidal crystals under similar constraints^{31, 34, 39}).

Application of the three order parameter set (S_2 , T_4 , C_4) to microscopy images (**Fig. 2**) demonstrates their quantification of different states including defects, spatial variations, and edge effects. For example, fluid states have vanishingly small values of all order parameters, and perfect crystals have nearly unity values for all order parameters. In contrast, nematic states have high nematic order, as expected, but also lower tetratic order and 4-fold connectivity that distinguish them from other states. The glassy state has low nematic and tetratic order, but relatively high 4-fold connectivity, where low orientational order is typical of glassy anisotropic particles, and high connectivity reflects the relatively higher coordination number. Although dynamic characterization is generally necessary to detect glassy behavior, static metrics for instantaneous states can be monitored as a function of time to serve as reaction coordinates.

Table 1. Reaction coordinate thresholds for state determination. Ranges for aspect ratio \sim 2 rounded rectangles based on ensemble average nematic, S_2 (Eq. (1)), tetratic, T_4 (Eq. (2)), and stretched four-fold connectivity, C_4 (Eq. (3)), based on prior hard particle simulations²⁶ and dipolar particle experiments.²⁷

state	particle orientational order	bond orientational order	
fluid (F)	S ₂ <0.5	<i>C</i> ₄ <0.6	
glassy (G)	S ₂ <0.5	<i>C</i> ₄>0.6	
nematic (N)	$S_2 > 0.5 \cap (S_2 - T_4) > 0.1$	C ₄ <0.85	
binematic (B)	$S_2 > 0.5 \cap S_2 - T_4 < 0.1$	<i>C</i> ₄ <0.85	
tetratic (T)	$T_4 > 0.5 \cap (S_2 - T_4) < -0.1$	<i>C</i> ₄ <0.85	
string fluid (Sf)	S ₂ >0.85	<i>C</i> ₄ <0.6	
smectic (Sm)	0.7< <i>S</i> ₂ <0.9	0.7< <i>C</i> ₄ <0.9	
crystal (X)	S ₂ >0.9	C ₄ >0.85	

Defining bounds of the three order parameters determines three-dimensional regions (**Table 1**) for each state (**Fig. 1**). Using the same red, yellow, blue coloring scheme for S_2 , T_4 , C_4 values of individual particles (**Fig. 2A**), we use a color mixing rule to indicate distinct 3D regions (**Fig. 2B**) for each state. Although the smectic state could be resolved by a single parameter specifically designed to detect smectic order, the current set of three order parameters defines a

Hendley et al. Page 6 of 22

region intermediate to nematic and crystal states, and is thus adequate for capturing this transient state. Other order parameters could be useful for tracking topological defects within confined liquid crystalline and crystalline states, which could also be connected to different local distortion profiles that control relaxation pathways.⁶⁵ In the context of our following results, we discuss how this order parameter set resolves assembly pathways and evolution between states.

Dynamic Pathways between Stable States

We now use the order parameters in **Table 1** as reaction coordinates to quantify dynamic pathways for transient stochastic microstructure evolution between states with changes in field mediated dipolar interactions. We first investigate transitions to stable states (**Fig. 3**) initiated from fluid states either with no field or weakly confined within low amplitude fields. Upon a step change in the electric field amplitude at fixed frequency, dipole-field interactions both align and compress particles into nematic (**Fig. 3A**) and crystal (**Fig. 3C**) states. Turning off or decreasing the field reversibly melts nematic (**Fig. 3B**) and crystal (**Fig. 3D**) states to low density fluid states. The field conditions and dipolar interactions that stabilize each initial and final state in **Fig. 3** are reported in **Table 2**. In the following, we discuss the reaction coordinate's ability to capture transient assembly pathways.

Table 2. Field conditions for initial and final states. Initial and final states are determined by field mediated dipolar interactions, which depend on field conditions. States are reported with AC electric field voltage, V, (that determines nonuniform field amplitude, $E_0 = V/d_g$) and frequency, ω , that together determine magnitudes of dipole-field⁵⁶ and dipole-dipole⁵⁷ interactions (see cited references for analytical potentials matched to measurements). Stable states are more directly linked to field conditions, whereas metastable states are approximate based on sensitivity to kinetics. Extended table available in supporting information.

state	V	ω/ MHz	dipole-field	orient / concentrate	dipole-dipole	chaining
F	0	0.3-20	zero	none / none	zero	none
N	0.3-2	0.3-5.5	low	med / med	low	low
Χ	1.8-2	0.3-1	med	high / high	med	high
G	1	2	low	low / med	low	low
BN	2-5	20	high	high / high	low	low
SF	1.5	0.4	low	low / low	high	high

Fluid-Nematic Pathway. We first discuss the case of starting from a homogeneous initial fluid state in the absence of any applied field, where we then make a step change to applied field parameters known to produce a stable nematic state (**Fig. 3A**, **Movie S1**).²⁷ Particles rapidly align with the field via a torque generated by an angular gradient in the dipole-field potential. The nematic director is the same as the field direction in lab coordinates. Particles translate towards the electrode central region (the electric field minimum) where they are compressed via the dipole-field potential and nonuniform field shape. ⁵⁶⁻⁵⁷ Particles translate to stable positions more slowly than they orient into alignment with the field, which aids formation of the nematic state during compression without many misoriented particles. Within ~10 min. of the field step change, all three coordinates stabilize at (S_2 , T_4 , C_4) \approx (0.75, 0.6, 0.75), which is a highly ordered nematic state without the positional order of a crystal or the biaxial order of binematic or tetratic states.

Images at different time points and video (**Movie S2**) colored by S_2 show how reaction coordinate trajectories capture the nematic ordering process. The 3D reaction coordinate trajectory (*i.e.*, S_2 , T_4 , C_4) colored by the mixing rule described in **Fig. 2** occurs along a manifold that is reproducible with many realizations of the same step change experiment in **Fig. 3A**. The transition from an initial homogeneous fluid to a nonuniform nematic state is continuous with an

Hendley et al. Page 7 of 22

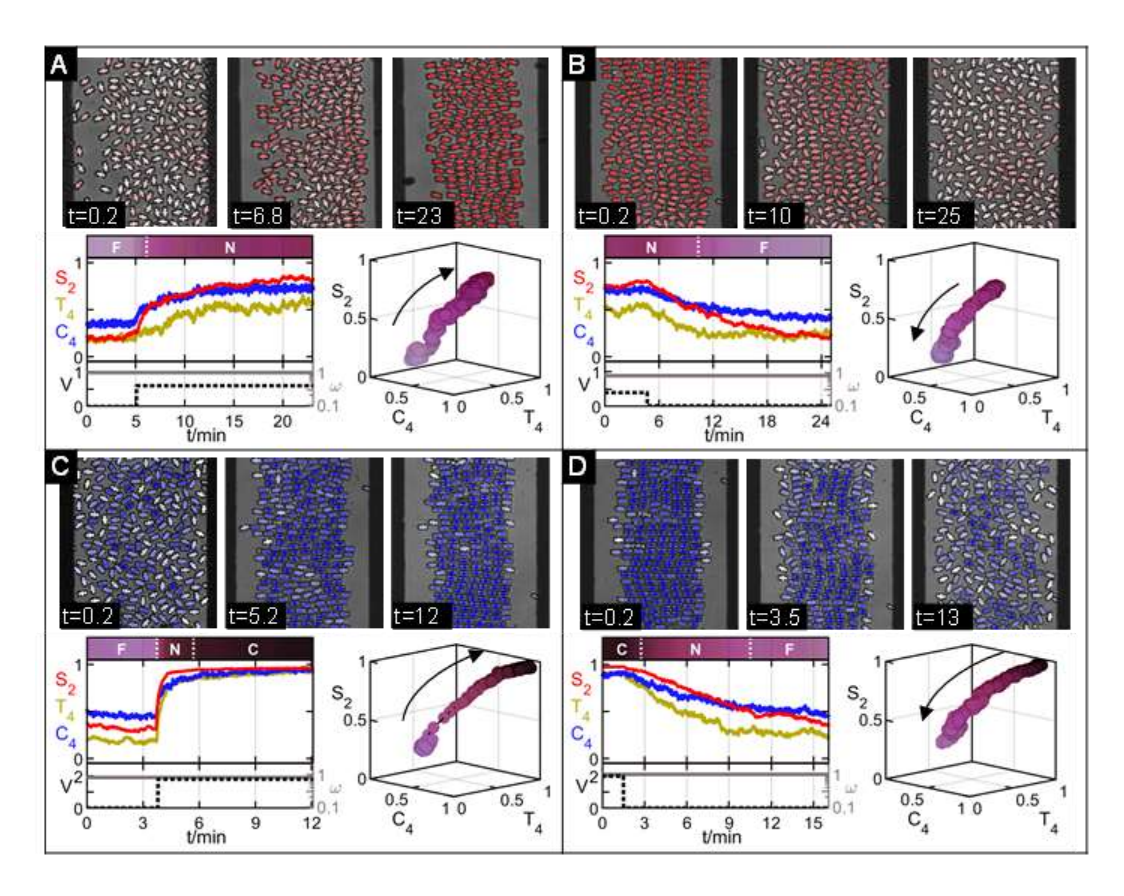


Fig. 3. Reversible dynamic pathways for fluid-nematic and fluid-nematic-crystal transitions of rectangular prisms in AC electric fields. State transitions for (A) fluid-nematic, (B) nematic-fluid, (C) fluid-crystal, and (D) crystal-fluid. In top of each panel, time-stamped microscopy images are colored by dominant reaction coordinates, including (A, B) $S_{2,i}$ and (C, D) $C_{4,i}$. Dark edges show 100 μ m electrode gap providing internal scale bar in addition to $2r_x = 8.4\mu$ m long particles. In lower-left of each panel, time dependent trajectories are shown for field parameters (V, ω), reaction coordinates (S_2 , T_4 , C_4), and state identification from **Table 1**. In lower-right of each panel, 3D reaction coordinate trajectories are colored by mixing rule in **Fig. 2** with arrows indicating direction.

approximately exponential relaxation towards a stable state. The nearly exponential evolution along each coordinate, and assembly pathway manifold, upon a field step change is consistent with saturation of a driving force (due to a free energy gradient) against a constant dissipative force (due to hydrodynamic interactions). Modeling relaxation rates is beyond the scope of this study, but the observed exponential behavior is similar to reaction coordinate based dynamic pathways for spherical colloidal crystals in AC electric fields where such rates were modeled in detail.^{31, 34}

With a step change reversal of the field (**Fig. 3B**, **Movie S2**), the nematic melts to the fluid with all reaction coordinates decaying in~10 minutes along the same 3D manifold as the forward assembly process. Because the forward and reverse assembly processes follow similar trajectories, the mechanisms appear similar based on the time evolution of particle and bond orientational order. The melting process occurs via the diffusion limited particle translation and rotation, as there is no field contribution mediating particle migration (as in field driven colloidal crystal disassembly³⁷).

<u>Fluid-Crystal Pathway</u>. With an understanding of the fluid-nematic transition, we next investigate fluid-crystal (**Fig. 3C**, **Movie S3**) and crystal-fluid (**Fig. 3D**, **Movie S3**) transitions as they pass through nematic states. Particles are colored by their C_4 values to capture the evolution of local

Hendley et al. Page 8 of 22

four-fold connectivity. Although dipolar potentials can produce different crystal states compared to hard particles of the same shape (*e.g.*, spherical dipolar colloidal crystals^{14, 66}), here rounded rectangles form crystals with stretched four-fold symmetry for both hard and dipolar potentials.²⁶⁻²⁷ As a result, C_4 is an appropriate reaction coordinate to capture local crystallinity. As with the fluid-nematic transition, we plot 3 separate reaction coordinates vs. time and the 3D trajectories.

With a step change in field parameters to conditions where the crystal is the stable state (**Table 2**), via stronger field mediated compression than the nematic, all three coordinates exponentially rise to near unity values (**Fig. 3C**). Local nematic order increases fastest to produce an intermediate nematic state that persists for several minutes before the onset of a crystal state characterized by $C_4>0.85$. This behavior is again attributed to the dipole-field potential driving faster rotation than translation at these field conditions (2V, 1MHz). This process shows an accessible dynamic assembly pathway where nematic ordering occurs with minimal misoriented particles; this provides a useful transition state along a pathway towards a low-defect crystal state. It does not appear possible to pass directly from the liquid to the crystal state without passing through a nematic state (although lower aspect ratio particles could instead pass through a rotator crystal state, 26 at a frequency where dipolar alignment is less favorable 56). It is possible that the assembly trajectory passes through a short-lived transient smectic state with both particle and bond orientational order exceeding what is expected in the nematic state but short of the crystal state.

The reverse melting process occurs along the same manifold in the 3D reaction coordinate space, passing through an intermediate nematic state, and possibly a transient smectic state (**Fig. 3D**, **Movie S4**). The decay rate of positional and orientational order occurs via diffusion limited melting of the crystal into the nematic and subsequently fluid states. The evolution of reaction coordinates during freezing and melting appears similar in that nematic order is greater than 4-fold bond orientational order, and both are greater than tetratic order. Bond orientational order correlates with positional ordering that changes during freezing and melting; this is consistent with C_4 rising the slowest during freezing and decaying first during melting. In short, orientational order already present in the nematic state continues to rise during freezing faster the positional order that defines the crystal states, and the melting process follows the same steps in reverse.

Dynamic Pathways between Metastable States

In addition to navigating between stable states, we explore the ability to navigate between non-equilibrium metastable states. Such states could include undesirable kinetically trapped states, transition states along pathways between stable states, or desirable configurations with exceptional mechanical, optical, electrical, or other properties. In the following, we explore assembly of initial fluid states into amorphous dynamically arrested glassy states, string fluids, and defective nematic states (binematics⁶⁰). By understanding accessible pathways between such metastable states, we can understand how to navigate toward or around such states as desired in different applications.

Fluid-Glassy State Pathway. We start by considering a quench of a dense fluid state into an arrested glassy state (**Fig. 4A**, **Movie S5**). By quenching a high density fluid, in contrast to a low density fluid (**Fig. 3A**), particles are compressed into a state that lacks orientational or positional order like the dense fluid, but is also unable to relax via self-diffusion or orient via dipole-field interactions. The S_2 and T_4 reaction coordinates for uniaxial and biaxial orientational order show little evolution after the step-change. A small increase in orientational order, S_2 , occurs via edge particle rotation that is less constrained than interior particles, although it is small and does not appear to spatially propagate into the interior on the observation time scale. The local 4-fold connectivity, C_4 , has the

Hendley et al. Page 9 of 22

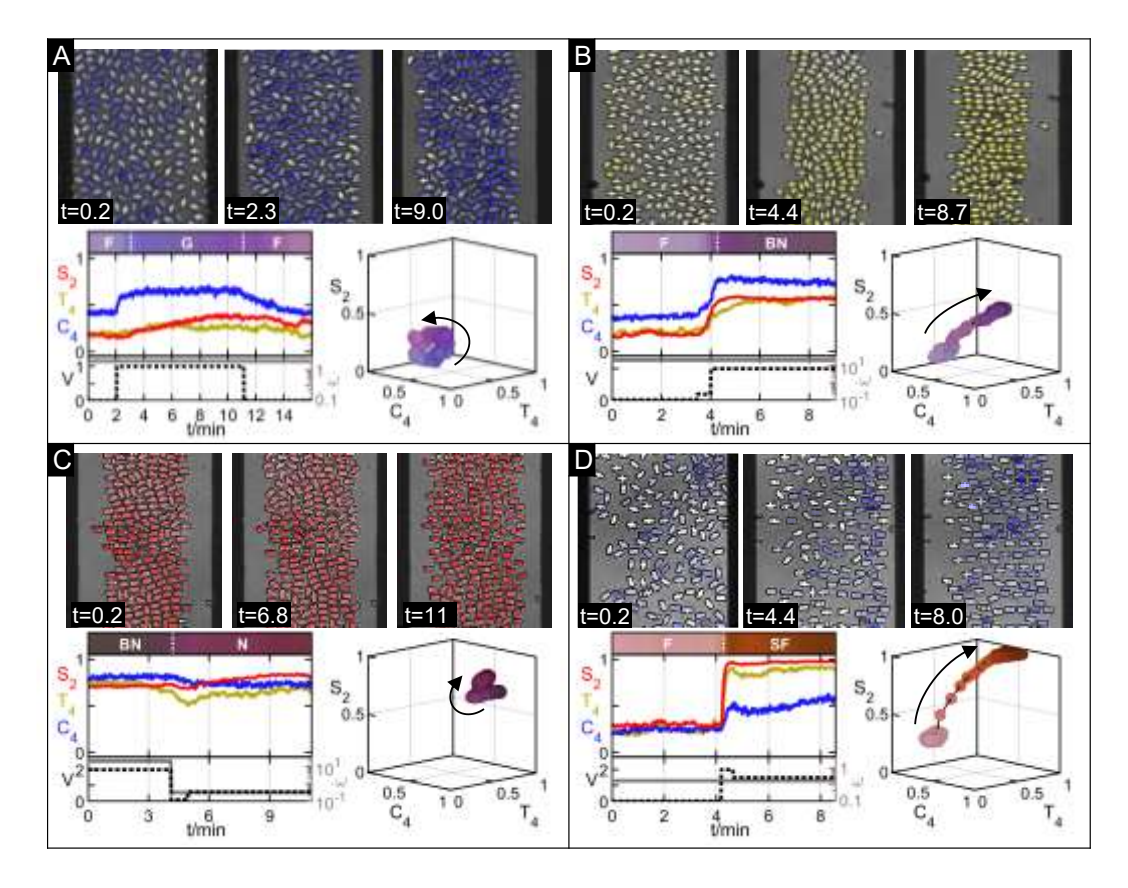


Fig. 4. Dynamic pathways between metastable states: fluid-glassy, fluid-binematic, binematic-nematic, and fluid-string transitions of rectangular prisms in AC electric fields. State transitions for (A) fluid-glassy state, (B) fluid-binematic, (C) binematic-fluid, and (D) fluid-string fluid. In top of each panel, time-stamped microscopy images are colored by dominant reaction coordinates, including (A, D) $C_{4,i}$, (B) $T_{4,i}$, and (C) $S_{2,i}$. Dark edges show 100 µm electrode gap providing internal scale bar in addition to $2r_x = 8.4$ µm long particles. In lower-left of each panel, time dependent trajectories are shown for field parameters (V, ω), reaction coordinates (S_2 , T_4 , C_4), and state identification from **Table 1**. In lower-right of each panel, 3D reaction coordinate trajectories are colored by mixing rule in **Fig. 2** with arrows indicating direction.

largest change with the field change. The local increase in bond orientational order and coordination number does not coincide with any long-range positional order, but is consistent with high local densities that lead to both rotational and translational arrest. The lack of orientational and positional order, together with an absence of long-time rotational or translational diffusive motion, leads us to characterize this as a glassy state. We do not further investigate ageing of this state, but plan in future work to characterize both its dynamic and structural features for comparison to other 2D anisotropic particle glassy states. 44,67

Upon field removal, the glassy configuration relaxes to a fluid state, but along a modified pathway compared to the one along which states initially formed. Practically, the 4-fold connectivity, C_4 , returns to a more typical fluid value as particles begin experiencing rotational and translation diffusion in a dense fluid state. However, orientational order, primarily of the edge particles, decays more slowly than bond orientational order with the field removal; this causes the disassembly trajectory to follow a path toward a high density fluid with initially more orientational order that ultimately decays to the initial dense fluid starting coordinates. As a result, the 3D reaction coordinate trajectory shows a hysteresis via the different assembly and disassembly

Hendley et al. Page 10 of 22

trajectories. Such a hysteresis could be exploited in annealing processes to produce desirable net state changes after many cycles, where for example, in the present case, it may be possibly to achieve glassy states with progressively more orientational order via cycling.

The glassy state does not appear to be easily reconfigured into nematic or crystal states without first returning to fluid states, which suggests the pathway from the fluid is a dead end. As such, we can target glassy states via the demonstrated pathway if their amorphous arrested configuration has desirable mechanical or electromagnetic scattering properties. However, reconfiguring the glassy state into nematic, crystal, or other states appears to require returning to a fluid state along a similar manifold, before sequentially choosing pathways towards other configurations. Although static magnetic fields have transformed low-density multi-domain nematics into more globally ordered nematics, ⁵² we are unaware of any precedent for relaxing a glassy state of anisotropic colloids into more ordered states via applied fields. After establishing the dead end pathway to the glassy state, we next explore pathways to other metastable states.

<u>Fluid-Binematic Pathway</u>. The fluid state can also be transformed into binematic states, ⁶⁰ where some fraction of particles are approximately orthogonal to the majority of particles aligned along a nematic director. The small fraction of misoriented particles in the binematic are effectively defects in an otherwise single domain nematic state. Larger system sizes can form multi-domain nematics where the local director continuously varies, or tetratic states as a sort of "patchwork" of local domains with biaxial orientational order. However, these states are not generally observed for relatively small slit pore geometries (small width compared to particle dimensions)⁶⁸⁻⁷⁰ like the confining parallel electrodes in this work.

To probe the fluid-binematic pathway, we start from an isotropic fluid, and then apply a high frequency (20MHz) field, which only weakly aligns particles with the field but rapidly concentrates particles at the electrode gap center (field minimum) (**Fig. 4B**, **Movie S6**). At this frequency (**Table 2**), translation is faster than rotation, which traps some single particles and small collections of vertically oriented particles, producing partial biaxial alignment. Since the fluid state has particles in all orientations, some particles are already orthogonal to the field direction and more likely to get trapped upon compression. Compared to the fluid-nematic transition, the reaction coordinate trajectories show significantly decreased local nematic order, S_2 , and increased local tetratic order, S_2 , producing the binematic state (**Table 1**). The decreased S_2 and increased S_3 are together produce a 3D reaction coordinate pathway toward a metastable terminus at the binematic state that follows a different manifold than the fluid-nematic pathway.

The formation of the binematic state (Fig. 4B, Movie S6) contrasts the assembly of the nematic (Fig. 3A) and glassy (Fig. 4A) states in several important ways. On the fluid-binematic path, we start at a lower initial fluid density than in the case where we quench to the glassy state (Fig. 4A), and also with less pre-alignment than in the fluid-nematic transition (Fig. 3A). The lower concentration, less pre-ordering, and weak field alignment produce the observed binematic order, or defective nematic order, which appears to emerge from coupled translation and rotation during compression. The binematic state is stable on observation times of at least tens of minutes, which suggest a significant barrier to relaxation; however, the binematic state is expected to be metastable with respect to the nematic state and ultimately relax via translation-rotation of misoriented particles. Rather than characterize relaxation at fixed conditions, we next explore changing field conditions to promote transition of binematic states to the other states.

Binematic-Nematic Pathway. We now investigate transition pathways accessible from the

Hendley et al. Page 11 of 22

binematic state. The reverse diffusion limited binematic-fluid transition along the same manifold as the assembly process is possible as in other cases studied so far. We were unable to produce a direct transition of the binematic into either glassy or crystal states without first passing through other states. In brief, stronger field mediated compression produces a quenched binematic state with similar orientational and positional order, where misoriented particles are not resolved. We were also unable to directly produce an arrested glassy state with no positional or orientational order without first passing through a dense fluid state. States having high tetratic order characteristic of a bulk tetratic phase were not routinely encountered except for transient microstructures like the one shown in **Fig. 1D**, which is perhaps not unexpected for small system sizes.^{26, 59} However, we were able to repeatedly produce relatively defect free nematic states from binematic states, so we focus on this pathway.

Using our prior knowledge of how field amplitude and frequency together control anisotropic particle orientation and localization at field minima (**Table 2**), $^{27, 56-57}$ we devised an approach to enable a transition from a metastable binematic state to a stable nematic state (**Fig. 4C**, **Movie S7**). Beginning with the field parameters that produce the metastable binematic state, the transition is initialized by slightly decreasing field amplitude to reduce compression at the electrode gap center, and then quickly before any occurrence of fluidization into an isotropic state, the field parameters to produce a stable nematic are re-applied (*i.e.*, the amplitude and frequency used to generate the nematic from the fluid state in **Fig. 3A**). The two-step process first allows relaxation of kinetically constrained particles, then subsequently drives orientational order to obtain the nematic state (where the dipole-field potential always drives nematic order over tetratic order). The 2D and 3D reaction coordinate trajectories first show decreasing tetratic and 4-fold bond orientational order, and then a subsequent increase in nematic order, S_2 , while T_4 and C_4 remain lower. This demonstrates an alternate pathway to the nematic state.

Fluid-String Fluid Pathway. Starting from a low density fluid, we demonstrate a transition to a "string fluid" state 14-15 where particles assemble into "strings" with orientational order aligned with the field direction, and with positional order along their length, but otherwise fluid based on their translational diffusion (Fig. 4D, Movie S8). This state is achieved via strong dipole-dipole interactions that align particles head-to-tail while simultaneously having minimal dipole-field mediated compression that would yield crystalline states. This combination of field mediated dipolar interactions is achieved by operating near to the positional cross-over frequency (0.3MHz) where the particle-field potential vanishes such that particles don't have a significant preference for the field minimum or maximum, 56 but the dipole-dipole potential is still determined by the field amplitude. Ellipsoids in AC electric fields have shown staggered chain stacking due to the angular dependence of dipolar potentials, 46 however, the rectangular particle corners do not allow sampling of the same relative angles between particles, so they simply stack head to tail.

The reaction coordinates for the fluid-string fluid transition capture rapidly increasing orientational order via S_2 , which also produces increasing tetratic order, but C_4 remains low due to low coordination and 4-fold bond orientational order. The 3D trajectory has less blue color than the transitions from the fluid glassy, nematic, and binematic states. The state is metastable in that "string" diffusion to enable string-string interactions is slow, and dipolar repulsion between strings does not allow them to coalesce as concentrated particles do under strong compression, **Fig. 3C**). The reverse process, at the same field frequency as the forward process, allows translational and rotational diffusion of particles so that the relatively dilute strings rapidly disassemble into a dilute fluid state along the same assembly pathway. By going to a different field frequency that favors

Hendley et al. Page 12 of 22

concentration of particles at the electric field minimum, it is possible to transition string fluids into nematic and the crystal states, although with fewer particles given the dilute fluid starting state.

Dynamic Pathway Map & State Reconfiguration

With an understanding of transition pathways between stable, metastable, and transient states, we demonstrate reconfiguration between states along the pathways identified in the 3D reaction coordinate space. To formulate the reconfiguration strategy more clearly in the context of dynamic pathways, we first summarize a "map" of available pathways (Fig. 5A, B) connecting states in the defined 3D coordinate space (Figs. 1D, 2B). For example, results in Figs. 3, 4 show the fluid state can be reversibly transformed into glassy, binematic, nematic, or string fluid states through careful control of initial conditions and field parameters. Accessing the crystal state requires passing through a highly ordered nematic state. States with high orientational and positional order such as crystals and string fluids can be disassembled through transient smectic states and into stable nematic states. Binematic states can be irreversibly transformed into nematic states, and glassy states are a dead end pathway that can only be disassembled into fluid states. Tetratic states are a low probability metastable state that can be considered a special case of the binematic state. Obtaining nearly infinite dilute configurations of non-interacting particles requires using electro-osmotic flows to remove particles from the electrode gaps.⁶³

With knowledge of how changes in electric field parameters determine the assembly of such diverse microstructures, and the dynamic transitions between microstructures, we can formally design, control, and optimize reconfiguration between accessible states along dynamic pathways defined by reaction coordinates. As noted in the introduction, such states can have exceptional optical, electrical, mechanical, thermal, and other properties, so reconfiguration between such states can enable active materials and devices. In the following, we demonstrate reconfiguration between different states based on navigating along available pathways with consideration of rate limiting dynamic processes that determine reconfiguration timescales. The following examples of field mediated reconfiguration are conducted using open-loop control schemes designed by a human agent based on domain expertise, but this scheme provides a basis to consider development of closed-loop control policies using theoretical and machine learning enabled approaches. ^{29, 31, 33}

<u>Fluid-Nematic-Crystal Reconfiguration</u>. We first demonstrate reconfiguring between fluid, nematic, and crystal states (**Fig. 5C**, **Movie S9**). From an initial fluid state, we are able to easily generate an intermediate nematic state as in **Fig. 3A**, which we transition directly to a crystal state. We could have easily reversed this process along the same 3D manifold back to the fluid state, but we decided to investigate switching between nematic and crystal states, which could be useful in device responses (*e.g.*, structural color displays⁷¹) based on material properties associated with such microstructures (*e.g.*, polarized iridescence⁷²⁻⁷³), but also for understanding basic questions about annealing crystals by cycling nematic-crystal transitions. Although a number of studies have explored the reversible dynamics of field mediated fluid-nematic transitions, ⁵³⁻⁵⁴ we are unaware of studies of nematic-crystal transitions with cycling.

Upon initial field application to generate the crystal state (**Fig. 5C**), the nematic transitions to the crystal along a path with higher 4-fold bond orientational order than nematic order $(C_4 > S_2)$, which differs slightly from the fluid-crystal manifold in **Fig. 3C** where $(C_4 < S_2)$. The primary difference between the two processes is the field step change (**Fig. 3C**) produces nematic order faster than 4-fold connectivity, whereas the slow ramp (**Fig. 5C**) produces 4-fold connectivity

Hendley et al. Page 13 of 22

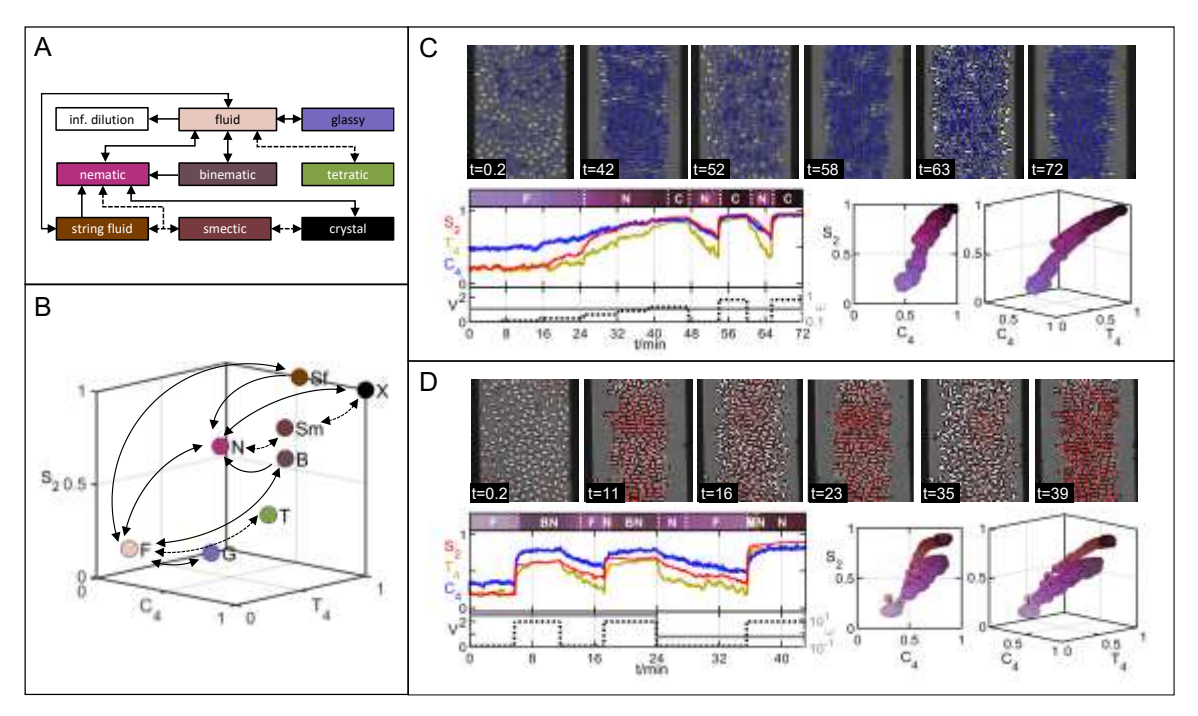


Fig. 5. Dynamic pathway map and reconfiguration between stable and metastable states. Pathways indicated (**A**) schematically and (**B**) by lines along manifolds in 3D reaction coordinate space. Arrows indicate favored direction as well as reversibility. State coloring scheme same as **Fig. 2**. Right panels show multiple reconfigurable transitions between (**C**) fluid-nematic-crystal states, and (D) fluid-binematic-nematic states. In top of each panel, time-stamped microscopy images are colored by dominant reaction coordinates, including (C) $C_{4,i}$, and (**D**) $S_{2,i}$. Dark edges show 100 μm electrode gap providing internal scale bar in addition to $2r_x = 8.4$ μm long particles. In lower-left of each panel, time dependent trajectories are shown for field parameters (V, ω), reaction coordinates (S_2 , T_4 , C_4), and state identification from **Table 1**. In lower-right of each panel, 3D reaction coordinate trajectories are colored by mixing rule in **Fig. 2**.

faster than nematic order. The slow ramp enhances dipole-field alignment and nematic order to bypass binematic states, which enhances evolution of 4-fold bond orientational order even before the threshold is passed to attain the crystal state (**Table 2**).

The resulting highly ordered crystal state has a small percentage of misoriented particles, which could arise from thermal fluctuations in the stable configuration, or as trapped defects, so we explore cycling between the nematic and crystal state in two more cycles. A reduction in the applied field amplitude reduces both dipolar alignment and compression so that particles return to a nematic state with a closely coupled decrease in both particle and bond orientational order. The increased translational and rotational diffusion of particles in the nematic state enables misoriented particles upon re-application of the higher voltage to become correctly oriented, which also enables improved positional order in the crystal state. Cycling the field two times produces a crystal state with exceptional order in terms of the 3D reaction coordinates (S_2 , T_4 , C_4) approaching (1,1,1). The crystal state displays some lattice variations that we attribute to thermal fluctuations due to its low modulus and small system size, but otherwise this configuration displays exceptional positional and orientational order. As a result, the original misoriented particles appear to be metastable defects trapped on the first compression that can be corrected with annealing, rather than defects due to thermal fluctuations in the crystal state.

<u>Fluid-Binematic-Nematic Reconfiguration</u>. We next demonstrate reconfiguring between states of varying orientational order including fluid, binematic, and nematic states (**Fig. 5D**, **Movie S10**).

Hendley et al. Page 14 of 22

Our results show the binematic state reproducibly assembled in nearly instantaneous field step changes, maintained as a metastable state, and then disassembled via diffusion limited processes into fluid states. This is shown two times with similar reaction coordinate pathways. After two cycles to the binematic state, we demonstrate a final quench with a lower frequency field to form a highly oriented nematic state. This last step shows the ability to form highly ordered states without memory of previously sampled disordered metastable states.

Reconfiguration between fluid, binematic, and nematic states demonstrates the informed choice of field parameters (global thermodynamic variables) that determine underlying energy landscapes and microstructure evolution along different dynamic pathways. For example, the initial quench to a specific combination of AC electric field amplitude and frequency produces compression of induced dipoles at the field minimum with less dipole-field alignment. This process reproducibly yields binematic states from fluid states along the same pathway (see 3D plot, Fig. 5D). In contrast, choosing a different field frequency more strongly, and quickly, aligns induced dipoles with the field, while also simultaneously undergoing compression at the field minimum. This slightly different process yields a different outcome to produce a highly ordered nematic along a different pathway (on a different landscape). The sensitivity of reconfiguration pathways between different states clearly demonstrates the selection of field parameters (Table 2) dictates reaction coordination manifolds on significantly different free energy landscapes. It follows that knowledge of these pathways is a necessary requirement to control navigation between states via thermodynamically and kinetically feasible reconfiguration processes.

Beyond knowledge of feasible pathways between states, reconfiguration rates/time scales (Figs. 5C,D) are determined by underlying landscapes features along pathways. Practically, the non-equilibrium stochastic evolution of structures depend on the drift and diffusion of the reaction coordinate trajectories determined by free energy and diffusivity landscapes (coefficients of lowdimensional Smoluchowski and Langevin equations, as quantified in previous studies of coarse grained colloidal assembly processes^{31, 34, 39, 41}). Here, we do not perform either the extensive measurements to obtain sufficient statistics or the necessary numerical analyses to obtain quantitative estimates of landscape features, which can be used to provide subsequent quantification of temporal reconfiguration information (e.g., transition rates, first passage times³¹, ³⁴). The kinetic data in **Figs. 3-5** generally show diffusion limited assembly upon step field changes to condensed states with rapid ordering and upon field removal slower loss of orientational and position order. However, defect relaxation within states (e.g., misoriented particles, vacancies, grain boundaries) occurs more slowly via cooperative processes, and these dynamics depend on detailed landscape features. As a result, state reconfiguration as part of materials processing or device performance will have dynamic responses determined by the time evolution on landscapes depending on different field conditions. Understanding the available pathways and their dynamics provide a basis to implement open and closed loop control of such reconfiguration processes (based on pathway navigation^{28, 30, 32}), which we plan to explore in future work.

Conclusions & Outlook

Our results demonstrate the controlled assembly and reconfiguration of rectangular prism particles between multiple quasi-2D configurations with liquid, liquid crystalline, and crystalline order. By tuning dipolar potentials mediated by AC electric field amplitude and frequency, we controlled the diffusion limited assembly and reconfiguration of stable liquid, nematic, and crystalline states, as well as metastable glassy, binematic, and string fluid states. We developed three reaction coordinates based on order parameters for rectangular prism particles that define

Hendley et al. Page 15 of 22

each state and dynamic pathways between states. Time dependent reaction coordinate trajectories show how orientational and positional order are coupled and collectively emerge in assembly processes and vanish in disassembly steps as we tune field conditions that mediate dipole-field and dipole-dipole potentials. Our results show it is possible on the order of minutes to transition between all states reversibly and repeatedly, which is practically useful for viable materials processing times and some device response rates.

Identification of manifolds within the three-coordinate space indicates the accessibility, reversibility, and rate of transitions along pathways between stable, metastable, and transient states. The resulting dynamic pathway map provides essential information to navigate between states in an informed manner to target desired states, avoid undesirable states, and optimize the rate of change between states. For example, a glassy state can be considered as a desirable target based on its amorphous microstructure and associated mechanical properties, but it can also be an undesirable dead-end state if a crystalline state is instead targeted for its diffractive properties. Likewise, the kinetically fastest route to a perfect crystal likely involves passing through an ordered nematic transition state, where orientational defects along other pathways are more slowly relaxing. Based on these findings, there is significant opportunity to further maximize the assembly and reconfiguration times through optimal control methods and additional field mediated actuation and control authority. 28, 30, 32 Because rectangular particle anisotropy and corners contribute to increased states, defects, and dynamical complexity compared to other 2D shaped particles, ^{26-27, 34} our findings related to achieving multiple target structures are expected to be translatable to selfassembly of other 2D particle based materials. In addition, our findings related to multi-state transitions involving liquid-glass, liquid-liquid crystal, and liquid crystal-crystal transitions have conceptually general features that can be applied to self-assembly in diverse materials and processes. Ultimately, knowledge of dynamic pathways in particle systems can be used to engineer assembly and reconfiguration of materials and devices based on self-organizing building blocks. Future work could further extend the approaches reported here to enable real-time feedback control over such processes that are effective without human intervention.

Materials & Methods

Particle Fabrication. Rounded rectangular prism (superelliptical prism) epoxy particles were fabricated using photolithography based on literature methods⁷⁴ adapted for particles with suitable charge for use in AC electric fields.⁵⁶⁻⁵⁷ In brief, Omnicoat (MicroChem) and SU-8 2002 (MicroChem) were sequentially spin coated at 3000 rpm on a silicon wafer. A photomask was used to pattern particles under a UV exposure energy of 60 mJ/cm². Particle dimensions were measured using a laser scanning microscope (Keyence). Particles were removed from the substrate with Remover PG (MicroChem), rinsed with isopropyl alcohol, and dispersed in deionized water. Particles were washed with 50% sulfuric acid to increase surface charge to prevent aggregation and deposition and produce enhanced induced dipoles in AC electric fields.⁵⁶⁻⁵⁷

Microscopy & Particle Tracking. The optical microscopy cell was similar to previous studies.^{27, 56-57, 63} An O-ring (McMaster-Carr) was placed on interdigitated gold electrodes (300 µm wide electrodes with a gap distance, d_g =100 µm) on a glass slide. The particle dispersion was pipetted into the O-ring and sealed to give area concentrations yielding ~140-220 particles in the imaging window. Electrodes were connected to a function generator (Agilent 33220A) to apply sinusoidal AC fields with peak-to-peak voltage, V, frequency, ω , and field amplitude, E_0 =V/ d_g , in an analytical expression for the spatially nonuniform field.⁵⁶ Particles were imaged in an inverted

Hendley et al. Page 16 of 22

microscope (Zeiss) with a 40x objective. Videos were captured at 5 frames/s using a CCD camera (Hamamatsu, Orca-ER) and Streampix (Norpix) software. Particle centroid position (x,y) and long-axis orientation (θ) were tracked using MATLAB algorithms.⁵⁶

Reaction Coordinates. Reaction coordinates, or order parameters vs. time, were computed from particle coordinates to quantify microstructure in microscopy images and videos. Details of computing each parameter are closely related to calculation of global order parameters described in detail in prior work, ²⁶⁻²⁷ but here we use local order parameters determined for each particle. For each local order parameter, an effective global parameter was obtained as an average over all particles in a configuration. The local nematic order for particle, *i*, was determined as, ⁷⁵⁻⁷⁶

$$S_{2,i} = \max_{\theta_{2,i}} \left\langle \cos\left(2\left(\theta_{j} - \theta_{2,i}\right)\right)\right\rangle_{j\left(r_{ij} < 6r_{x}\right)} \tag{1}$$

where r_{ij} , is center-to-center distance between particle *i* and neighboring particles *j* within six long axis radii, $6r_x$, and the local director direction, $\theta_{2,i}$, is calculated by maximizing the function. Local tetratic order was quantified by the maximum relative orientation to a bidirector, θ_4 , as, ^{59, 77}

$$T_{4,i} = \max_{\theta_{4,i}} \left\langle \cos\left(4\left(\theta_i - \theta_4\right)\right)\right\rangle_{j\left(r_{ij} < 6r_x\right)} \tag{2}$$

To quantify crystallinity, we characterized average four- $(\langle C_4 \rangle)$ or six- $(\langle C_6 \rangle)$ fold connectivity by averaging each particle's local value as,⁷⁸

$$C_{n,i} = \frac{1}{n} \sum_{j=1}^{N_{b,i}} \begin{bmatrix} 1 & \chi_n^{ij} \ge 0.32 \\ 0 & \chi_n^{ij} < 0.32 \end{bmatrix}, \quad \chi_n^{ij} = \frac{\left| \text{Re} \left[\psi_{n,i} \psi_{n,j}^* \right] \right|}{\left| \psi_{n,i} \psi_{n,j}^* \right|}$$
(3)

where the local stretched bond orientational order parameter, $\psi_{n,i}$ (and its complex conjugate, $\psi^*_{n,i}$), was recently defined in our prior work as,²⁶

$$\psi_{n,j} = \frac{1}{N_{b,j}} \left| \sum_{k=1}^{N_{b,j}} \exp(in\theta_{jk}) \right| = \frac{1}{N_{b,j}} \left| \sum_{k=1}^{N_{b,j}} \cos(n\theta_{jk}) + i\sin(n\theta_{jk}) \right|$$
(4)

where $N_{b,j}$ is the number of neighbors with bonds to particle j, and θ_{jk} is the angle between particle centers relative to an arbitrary axis.

Notes. The authors declare no competing financial interest. **Acknowledgments.** We acknowledge financial support from the National Science Foundation CBET-1928950. **Supporting Information.** Supporting information for this article including a table of experimental field conditions and a list of movies and their captions is available free of charge at http://pubs.acs.org.

References

- 1. Whitesides, G. M.; Grzybowski, B. Self-Assembly at All Scales. *Science* **2002**, *295*, 2418-2421.
- 2. Service, R. F. How Far Can We Push Chemical Self-Assembly? *Science* **2005**, *309*, 95-95.
- 3. Rohrdanz, M. A.; Zheng, W.; Clementi, C. Discovering Mountain Passes Via Torchlight: Methods for the Definition of Reaction Coordinates and Pathways in Complex Macromolecular Reactions. *Ann. Rev. Phys. Chem.* **2013**, *64*, 295-316.
- 4. Whitelam, S.; Jack, R. L. The Statistical Mechanics of Dynamic Pathways to Self-Assembly. *Annual Review of Physical Chemistry* **2015**, *66*, 143-163.

Hendley et al. Page 17 of 22

- 5. Peters, B. Reaction Coordinates and Mechanistic Hypothesis Tests. *Annual Review of Physical Chemistry* **2016**, *67*, 669-690.
- 6. Wales, D. J. Exploring Energy Landscapes. *Annual Review of Physical Chemistry* **2018**, *69*, 401-425.
- 7. Boles, M. A.; Engel, M.; Talapin, D. V. Self-Assembly of Colloidal Nanocrystals: From Intricate Structures to Functional Materials. *Chemical Reviews* **2016**, *116*, 11220-11289.
- 8. Vogel, N.; Retsch, M.; Fustin, C.-A.; del Campo, A.; Jonas, U. Advances in Colloidal Assembly: The Design of Structure and Hierarchy in Two and Three Dimensions. *Chemical Reviews* **2015**, *115*, 6265-6311.
- 9. Solomon, M. J. Tools and Functions of Reconfigurable Colloidal Assembly. *Langmuir* **2018**, *34*, 11205-11219.
- 10. Grant, M. C.; Russel, W. B. Volume-Fraction Dependence of Elastic Moduli and Transition Temperature for Colloidal Silica Gels. *Phys. Rev. E* **1993**, *47*, 2606-2614.
- 11. Bevan, M. A.; Petris, S. N.; Chan, D. Y. C. Solvent Quality Dependent Continuum Van Der Waals Attraction and Phase Behavior for Colloids Bearing Nonuniform Adsorbed Polymer Layers. *Langmuir* **2002**, *18*, 7845-7852.
- 12. Savage, J. R.; Blair, D. W.; Levine, A. J.; Guyer, R. A.; Dinsmore, A. D. Imaging the Sublimation Dynamics of Colloidal Crystallites. *Science* **2006**, *314*, 795-798.
- 13. Fernandes, G. E.; Beltran-Villegas, D. J.; Bevan, M. A. Interfacial Colloidal Crystallization *Via* Tunable Hydrogel Depletants. *Langmuir* **2008**, *24*, 10776-10785.
- 14. Yethiraj, A.; Blaaderen, A. v. A Colloidal Model System with an Interaction Tunable from Hard Sphere to Soft and Dipolar. *Nature* **2003**, *421*, 513-517.
- 15. Hynninen, A.-P.; Dijkstra, M. Phase Diagram of Dipolar Hard and Soft Spheres: Manipulation of Colloidal Crystal Structures by an External Field. *Phys. Rev. Lett.* **2005**, *94*, 138303-4.
- 16. Goyal, A.; Hall, C. K.; Velev, O. D. Phase Diagram for Stimulus-Responsive Materials Containing Dipolar Colloidal Particles. *Phys. Rev. E* **2008**, 77, 031401-6.
- 17. Park, S. Y.; Lytton-Jean, A. K. R.; Lee, B.; Weigand, S.; Schatz, G. C.; Mirkin, C. A. DNA-Programmable Nanoparticle Crystallization. *Nature* **2008**, *451*, 553-556.
- 18. Casey, M. T.; Scarlett, R. T.; Benjamin Rogers, W.; Jenkins, I.; Sinno, T.; Crocker, J. C. Driving Diffusionless Transformations in Colloidal Crystals Using DNA Handshaking. *Nature Communications* **2012**, *3*, 1209.
- 19. Ryan, J. N.; Elimelech, M. Colloid Mobilization and Transport in Groundwater. *Colloids and Surfaces A: Physicochemical and Engineering Aspects* **1996**, *107*, 1-56.
- 20. Mitchell, M. J.; Billingsley, M. M.; Haley, R. M.; Wechsler, M. E.; Peppas, N. A.; Langer, R. Engineering Precision Nanoparticles for Drug Delivery. *Nature Reviews Drug Discovery* **2021**, 20, 101-124.
- 21. Comiskey, B.; Albert, J. D.; Yoshizawa, H.; Jacobson, J. An Electrophoretic Ink for All-Printed Reflective Electronic Displays. *Nature* **1998**, *394*, 253-255.
- 22. Arpin, K. A.; Mihi, A.; Johnson, H. T.; Baca, A. J.; Rogers, J. A.; Lewis, J. A.; Braun, P. V. Multidimensional Architectures for Functional Optical Devices. *Adv. Mater.* **2010**, *22*, 1084-1101.
- 23. Saadi, M. A. S. R.; Maguire, A.; Pottackal, N. T.; Thakur, M. S. H.; Ikram, M. M.; Hart, A. J.; Ajayan, P. M.; Rahman, M. M. Direct Ink Writing: A 3d Printing Technology for Diverse Materials. *Advanced Materials* **2022**, *34*, 2108855.
- 24. Lu, J. P.; Thompson, J. D.; Whiting, G. L.; Biegelsen, D. K.; Raychaudhuri, S.; Lujan, R.; Veres, J.; Lavery, L. L.; Völkel, A. R.; Chow, E. M. Open and Closed Loop Manipulation of

Hendley et al. Page 18 of 22

- Charged Microchiplets in an Electric Field. Appl. Phys. Lett. 2014, 105, 054104.
- 25. Damasceno, P. F.; Engel, M.; Glotzer, S. C. Predictive Self-Assembly of Polyhedra into Complex Structures. *Science* **2012**, *337*, 453-457.
- 26. Torres-Díaz, I.; Hendley, R. S.; Mishra, A.; Yeh, A. J.; Bevan, M. A. Hard Superellipse Phases: Particle Shape Anisotropy & Curvature. *Soft Matter* **2022**, *18*, 1319-1330.
- 27. Hendley, R. S.; Zhang, L.; Bevan, M. A. Design Rules for 2d Field Mediated Assembly of Different Shaped Colloids into Diverse Microstructures. *Soft Matter* **2022**, *18*, 9273-9282.
- 28. ten Wolde, P. R.; Frenkel, D. Enhancement of Protein Crystal Nucleation by Critical Density Fluctuations. *Science* **1997**, *277*, 1975-1978.
- 29. Beltran-Villegas, D. J.; Bevan, M. A. Free Energy Landscapes for Colloidal Crystal Assembly. *Soft Matter* **2011**, *7*, 3280-3285.
- 30. Newton, A. C.; Groenewold, J.; Kegel, W. K.; Bolhuis, P. G. Rotational Diffusion Affects the Dynamical Self-Assembly Pathways of Patchy Particles. *Proceedings of the National Academy of Sciences* **2015**, *112*, 15308-15313.
- 31. Yang, Y.; Thyagarajan, R.; Ford, D. M.; Bevan, M. A. Dynamic Colloidal Assembly Pathways Via Low Dimensional Models. *J. Chem. Phys.* **2016**, *144*, 204904.
- 32. Mao, R.; O'Leary, J.; Mesbah, A.; Mittal, J. A Deep Learning Framework Discovers Compositional Order and Self-Assembly Pathways in Binary Colloidal Mixtures. *JACS Au* **2022**, *2*, 1818-1828.
- 33. Savage, J. R.; Dinsmore, A. D. Experimental Evidence for Two-Step Nucleation in Colloidal Crystallization. *Phys. Rev. Lett.* **2009**, *102*, 198302.
- 34. Edwards, T. D.; Yang, Y.; Beltran-Villegas, D. J.; Bevan, M. A. Colloidal Crystal Grain Boundary Formation and Motion. *Sci. Rep.* **2014**, *4*, 06132.
- 35. Perry, R. W.; Holmes-Cerfon, M. C.; Brenner, M. P.; Manoharan, V. N. Two-Dimensional Clusters of Colloidal Spheres: Ground States, Excited States, and Structural Rearrangements. *Physical Review Letters* **2015**, *114*, 228301.
- 36. Fang, H.; Hagan, M. F.; Rogers, W. B. Two-Step Crystallization and Solid-Solid Transitions in Binary Colloidal Mixtures. *Proceedings of the National Academy of Sciences* **2020**, *117*, 27927-27933.
- 37. Juarez, J. J.; Bevan, M. A. Feedback Controlled Colloidal Self-Assembly. *Adv. Funct. Mater.* **2012**, *22*, 3833-3839.
- 38. Bevan, M. A.; Ford, D. M.; Grover, M. A.; Shapiro, B.; Maroudas, D.; Yang, Y.; Thyagarajan, R.; Tang, X.; Sehgal, R. M. Controlling Assembly of Colloidal Particles into Structured Objects: Basic Strategy and a Case Study. *J. Process Control* **2015**, *27*, 64-75.
- 39. Tang, X.; Rupp, B.; Yang, Y.; Edwards, T. D.; Grover, M. A.; Bevan, M. A. Optimal Feedback Controlled Assembly of Perfect Crystals. *ACS Nano* **2016**, *10*, 6791-6798.
- 40. Zhang, J.; Yang, J.; Zhang, Y.; Bevan, M. A. Controlling Colloidal Crystals Via Morphing Energy Landscapes and Reinforcement Learning. *Science Advances* **2020**, *6*, eabd6716.
- 41. Beltran-Villegas, D. J.; Sehgal, R. M.; Maroudas, D.; Ford, D. M.; Bevan, M. A. Colloidal Cluster Crystallization Dynamics. *J. Chem. Phys.* **2012**, *137*, 134901.
- 42. Glotzer, S. C.; Solomon, M. J. Anisotropy of Building Blocks and Their Assembly into Complex Structures. *Nat Mater* **2007**, *6*, 557-562.
- 43. Wu, N.; Lee, D.; Striolo, A. Anisotropic Particle Assemblies. Elsevier: Amsterdam, 2018.
- 44. Liu, X.; Wang, H.; Zhang, Z.; Kosterlitz, J. M.; Ling, X. S. Nature of the Glass Transition in 2d Colloidal Suspensions of Short Rods. *New Journal of Physics* **2020**, *22*, 103066.
- 45. Zheng, Z.; Ni, R.; Wang, Y.; Han, Y. Translational and Rotational Critical-Like Behaviors in

Hendley et al. Page 19 of 22

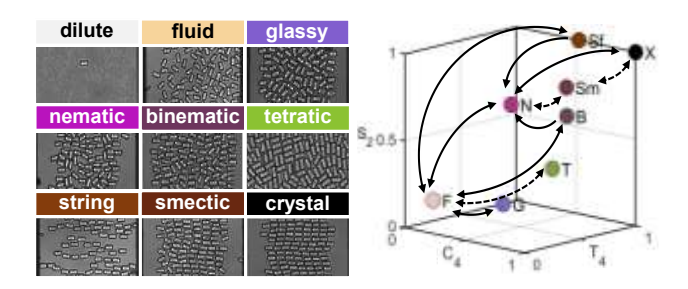
- the Glass Transition of Colloidal Ellipsoid Monolayers. Science Advances 2021, 7, eabd1958.
- 46. Singh, J. P.; Lele, P. P.; Nettesheim, F.; Wagner, N. J.; Furst, E. M. One- and Two-Dimensional Assembly of Colloidal Ellipsoids in Ac Electric Fields. *Physical Review E* **2009**, *79*, 050401.
- 47. Kuijk, A.; Troppenz, T.; Filion, L.; Imhof, A.; van Roij, R.; Dijkstra, M.; van Blaaderen, A. Effect of External Electric Fields on the Phase Behavior of Colloidal Silica Rods. *Soft Matter* **2014**, *10*, 6249-6255.
- 48. Stelson, A. C.; Penterman, S. J.; Liddell Watson, C. M. Electric Field-Directed Assembly of Fullerene Crystal Rods into Hierarchical Films. *Journal of Materials Chemistry C* **2018**, *6*, 11118-11127.
- 49. Wittmann, R.; Cortes, L. B. G.; Löwen, H.; Aarts, D. G. A. L. Particle-Resolved Topological Defects of Smectic Colloidal Liquid Crystals in Extreme Confinement. *Nature Communications* **2021**, *12*, 623.
- 50. Yao, X.; Zhang, H.; Chen, J. Z. Y. Topological Defects in Two-Dimensional Liquid Crystals Confined by a Box. *Physical Review E* **2018**, *97*, 052707.
- 51. Gârlea, I. C.; Mulder, B. M. Defect Structures Mediate the Isotropic-Nematic Transition in Strongly Confined Liquid Crystals. *Soft Matter* **2015**, *11*, 608-614.
- 52. Tan, X.; Chen, Y.; Wang, H.; Zhang, Z.; Ling, X. S. 2d Isotropic–Nematic Transition in Colloidal Suspensions of Ellipsoids. *Soft Matter* **2021**, *17*, 6001-6005.
- 53. Kao, P.-K.; VanSaders, B. J.; Durkin, M. D.; Glotzer, S. C.; Solomon, M. J. Anisotropy Effects on the Kinetics of Colloidal Crystallization and Melting: Comparison of Spheres and Ellipsoids. *Soft Matter* **2019**, *15*, 7479-7489.
- 54. Boehm, S. J.; Lin, L.; Guzman Betancourt, K.; Emery, R.; Mayer, J. S.; Mayer, T. S.; Keating, C. D. Formation and Frequency Response of Two-Dimensional Nanowire Lattices in an Applied Electric Field. *Langmuir* **2015**, *31*, 5779-86.
- 55. Pethig, R. *Dielectrophoresis: Theory, Methodology, and Biological Applications*. John Wiley & Sons, Inc.: Hoboken, NJ, **2017**.
- 56. Rupp, B.; Torres-Diaz, I.; Hua, X.; Bevan, M. A. Measurement of Anisotropic Particle Interactions with Nonuniform Ac Electric Fields. *Langmuir* **2018**, *34*, 2497-2504.
- 57. Hendley, R. S.; Torres-Díaz, I.; Bevan, M. A. Anisotropic Colloidal Interactions & Assembly in Ac Electric Fields. *Soft Matter* **2021**, *17*, 9066-9077.
- 58. Fejer, S. N.; Chakrabarti, D.; Wales, D. J. Self-Assembly of Anisotropic Particles. *Soft Matter* **2011**, *7*, 3553-3564.
- 59. Donev, A.; Burton, J.; Stillinger, F. H.; Torquato, S. Tetratic Order in the Phase Behavior of a Hard-Rectangle System. *Physical Review B* **2006**, *73*, 054109.
- 60. Sitta, C. E.; Smallenburg, F.; Wittkowski, R.; Löwen, H. Liquid Crystals of Hard Rectangles on Flat and Cylindrical Manifolds. *Physical Chemistry Chemical Physics* **2018**, *20*, 5285-5294.
- 61. Baron, P. B.; Hendley, R. S.; Bevan, M. A. Anisotropic Particle Multiphase Equilibria in Nonuniform Fields. *The Journal of Chemical Physics* **2023**, *159*.
- 62. Torres-Díaz, I.; Rupp, B.; Yang, Y.; Bevan, M. A. Energy Landscapes for Ellipsoids in Non-Uniform Ac Electric Fields. *Soft Matter* **2018**, *14*, 934-944.
- 63. Bahukudumbi, P.; Everett, W. N.; Beskok, A.; Huff, G. H.; Lagoudas, D.; Ounaies, Z.; Bevan, M. A. Colloidal Microstructures, Transport, and Impedance Properties within Interfacial Microelectrodes. *Appl. Phys. Lett.* **2007**, *90*, 224102.
- 64. Schoenholz, S. S.; Cubuk, E. D.; Kaxiras, E.; Liu, A. J. Relationship between Local Structure and Relaxation in out-of-Equilibrium Glassy Systems. *Proceedings of the National Academy of Sciences* **2017**, *114*, 263-267.

Hendley et al. Page 20 of 22

- 65. Zhang, R.; Kumar, N.; Ross, J. L.; Gardel, M. L.; de Pablo, J. J. Interplay of Structure, Elasticity, and Dynamics in Actin-Based Nematic Materials. *Proceedings of the National Academy of Sciences* **2018**, *115*, E124-E133.
- 66. Tao, R.; Sun, J. M. Three-Dimensional Structure of Induced Electrorheological Solid. *Phys. Rev. Lett.* **1991,** *67*, 398.
- 67. Zheng, Z.; Ni, R.; Wang, F.; Dijkstra, M.; Wang, Y.; Han, Y. Structural Signatures of Dynamic Heterogeneities in Monolayers of Colloidal Ellipsoids. *Nature Communications* **2014**, *5*, 3829.
- 68. Rodriguez, G.; Vicente, L. Density Profiles of Colloidal Suspensions in Equilibrium inside Slit Pores. *Molecular Physics* **1996**, *87*, 213-226.
- 69. van Roij, R.; Dijkstra, M.; Evans, R. Orientational Wetting and Capillary Nematization of Hard-Rod Fluids. *Europhysics Letters* **2000**, *49*, 350-356.
- 70. Geigenfeind, T.; Rosenzweig, S.; Schmidt, M.; Heras, D. d. l. Confinement of Two-Dimensional Rods in Slit Pores and Square Cavities. *The Journal of Chemical Physics* **2015**, 142, 174701.
- 71. Tittl, A. Tunable Structural Colors on Display. Light: Science & Applications 2022, 11, 155.
- 72. Sharma, V.; Crne, M.; Park, J. O.; Srinivasarao, M. Structural Origin of Circularly Polarized Iridescence in Jeweled Beetles. *Science* **2009**, *325*, 449-451.
- 73. McDougal, A.; Miller, B.; Singh, M.; Kolle, M. Biological Growth and Synthetic Fabrication of Structurally Colored Materials. *Journal of Optics* **2019**, *21*, 073001.
- 74. Hernandez, C. J.; Mason, T. G. Colloidal Alphabet Soup: Monodisperse Dispersions of Shape-Designed Lithoparticles. *The Journal of Physical Chemistry C* **2007**, *111*, 4477-4480.
- 75. Cuesta, J. A.; Frenkel, D. Monte Carlo Simulation of Two-Dimensional Hard Ellipses. *Phys Rev A* **1990**, *42*, 2126-2136.
- 76. Narayan, V.; Menon, N.; Ramaswamy, S. Nonequilibrium Steady States in a Vibrated-Rod Monolayer: Tetratic, Nematic, and Smectic Correlations. *Journal of Statistical Mechanics: Theory and Experiment* **2006**, *2006*, P01005-P01005.
- 77. Wojciechowski, K. W.; Frenkel, D. Tetratic Phase in the Planar Hard Square System? *J. Compit. Methods Sci. Eng.* **2004**, *10*, 235.
- 78. ten Wolde, P. R.; Ruiz-Montero, M. J.; Frenkel, D. Numerical Calculation of the Rate of Crystal Nucleation in a Lennard-Jones System at Moderate Undercooling. *J. Chem. Phys.* **1996**, *104*, 9932.

Hendley et al. Page 21 of 22

For Table of Contents Use Only
For Table of Contents Use Only (1.75 inches high x 3.25 inches wide)



Page 22 of 22 Hendley et al.